Available online at www.sciencedirect.com
ScienceDirect
Journal of Solid State Chemistry 180 (2007) 3058–3065
JOURNAL OF SOLID STATE CHEMISTRY
www.elsevier.com/locate/jssc

Enhanced photoluminescence of Ba_2GdNbO_6: Eu^{3+}/Dy^{3+} phosphors by Li^+ doping

C.C. Yu[a,b], X.M. Liu[a], M. Yu[a,b], C.K. Lin[a], C.X. Li[a], H. Wang[a], J. Lin[a,*]

[a]*State Key Laboratory of Application of Rare Earth Resources, Changchun Institute of Applied Chemistry, Chinese Academy of Sciences, Changchun 130022, PR China*

[b]*Department of Chemistry, Northeast Normal University, Changchun 130024, PR China*

Received 18 April 2007; received in revised form 7 August 2007; accepted 31 August 2007
Available online 11 September 2007

Abstract

The Ba_2GdNbO_6: Eu^{3+}/Dy^{3+} and Li^+-doped Ba_2GdNbO_6: Eu^{3+}/Dy^{3+} phosphors were prepared by solid-state reaction process. X-ray diffraction (XRD), field emission scanning electron microscopy (FE-SEM) and photoluminescence (PL) as well as lifetimes, was utilized to characterize the resulting phosphors. Under the excitation of ultraviolet light, the Ba_2GdNbO_6: Eu^{3+}/Dy^{3+} and Li^+-doped Ba_2GdNbO_6: Eu^{3+}/Dy^{3+} show the characteristic emissions of Eu^{3+} ($^5D_0$–$^7F_{1,2,3}$ transitions dominated by $^5D_0$–$^7F_1$ at 593 nm) and Dy^{3+} ($^4F_{9/2}$–$^6H_{15/2,13/2}$ transitions dominated by $^4F_{9/2}$–$^6H_{15/2}$ at 494 nm), respectively. The incorporation of Li^+ ions into the Ba_2GdNbO_6: Eu^{3+}/Dy^{3+} phosphors has enhanced the PL intensities depending on the doping concentration of Li^+, and the highest emission was obtained in $Ba_2Gd_{0.9}NbO_6$: $0.10Eu^{3+}$, $0.01Li^+$ and $Ba_2Gd_{0.95}NbO_6$: $0.05Dy^{3+}$, $0.07Li^+$, respectively. An energy level diagram was proposed to explain the luminescence process in the phosphors.

Keywords: Phosphor; Europium; Dysprosium; Photoluminescence; Niobate

1. Introduction

Inorganic compounds doped with rare earth ions form an important class of phosphors for many luminescence applications. Oxide-based luminescent materials have been widely used due to their thermal and chemical stability. Improved performance of displays requires high-quality phosphors for sufficient brightness and long-term stability. To enhance the luminescent characteristics of the phosphors, extensive research has been carried out on rare-earth-activated phosphors. Phosphors doped with Eu^{3+} give rise to red or red-orange emission, and those doped with Dy^{3+} mainly consist of narrow lines in the blue and yellow wavelength region and play an important role in emissive display technology, such as plasma display panel (PDP), field emission display (FED), and in the lighting industry, such as tricolor lamps [1–6]. Eu^{3+} is especially useful and commonly utilized as a probe of the local crystal field affecting RE^{3+}. Thus, it is known that the number of observed lines of the strong and easily recordable $^5D_0$–^7F_J ($J = 0, 1, 2$) emission allows differentiation between Eu^{3+} in locations with different site symmetries [7,8]. Unlike the most frequently used Eu^{3+} and Tb^{3+} (in oxide hosts), which have allowed charge-transfer absorption band (CTB) or $4f^8$–$4f^7 5d$ absorption band in the UV region, respectively, the excitation spectrum of Dy^{3+} consists of only narrow f–f transition lines from 300 to 500 nm (both CTB and $4f^9$–$4f^8 5d$ band of Dy^{3+} are located below 200 nm) [9]. As a result, the luminescence of Dy^{3+} cannot be excited with 254 nm UV light efficiently, and the excitation can occur only through the f–f transitions with low oscillator strength (10^{-6}) due to their forbidden features by the parity selection rule [10]. This drawback of Dy^{3+} luminescence can be overcome by sensitization, such as host sensitization in YVO_4: Dy^{3+} [11] and ion sensitization in $Ca_2Gd_8(SiO_4)_6O_2$: Pb^{2+}, Dy^{3+} [12].

Ba_2GdNbO_6 has a complex cubic perovskite ($A_2BB'O_6$) structure [13,14]. Much interest in Ba_2GdNbO_6 is driven by its possible applications of this material as a substrate of

*Corresponding author.
E-mail address: jlin@ciac.jl.cn (J. Lin).

0022-4596/$ - see front matter © 2007 Elsevier Inc. All rights reserved.
doi:10.1016/j.jssc.2007.08.028

high T_c superconductors [13,15]. So far only limited information is available on the rare earth ions (RE^{3+})-doped Ba_2GdNbO_6 phosphors. Blasse and Bril obtained luminescence spectra of the Eu^{3+} impurity in some compounds such as $Ba(Sb,Nb)_2O_6$ [16]. The energy distribution of the emission of Eu^{3+}-activated Ba_2GdNbO_6 show a sharp line at 593 nm corresponding to the $^5D_0$–$^7F_1$ transition without detailed explanation for the luminescence mechanism [17].

Charge compensating plays an important role in improving the luminescence efficiency of phosphors. It has been reported that a charge-compensated phosphor is brighter than that of uncompensated phosphors [18–20]. Li^+ co-doping helps to incorporate Eu^{3+}, Dy^{3+} into lattice sites by increasing the crystallinity. Several groups have investigated the effect of Li^+ substitution on the luminescent properties of $SrTiO_3$: Pr^{3+} and Gd_2O_3: Eu^{3+} [21,22]. These studies showed that the incorporation of Li^+ ions into the phosphors may greatly enhance the luminescence efficiently even in a small quantity [23–25]. Accordingly, we select Eu^{3+} and Dy^{3+} as activators in Ba_2GdNbO_6 host in order to reveal the relationship between their emission properties and the host structure, and to enhance their emission intensity by Li^+ doping for lighting application. Detailed synthesis and luminescence characterization of the Ba_2GdNbO_6: Eu^{3+}/Dy^{3+} and Li^+-doped Ba_2GdNbO_6: Eu^{3+}/Dy^{3+} samples are reported.

2. Experimental

The phosphor samples Ba_2GdNbO_6: Eu^{3+}/Dy^{3+} and the corresponding Li^+-doped Ba_2GdNbO_6: Eu^{3+}/Dy^{3+} were synthesized using a high temperature solid-state reaction technique. The starting materials were Gd_2O_3, Eu_2O_3, Dy_2O_3 (all 99.99%, shanghai Yuelong Non-Ferrors Metals), Nb_2O_5, $LiNO_3$, $Ba(NO_3)_2$ (analytical reagent, A. R., Beijing Fine Chemical Company). The doping concentrations of Eu^{3+}, Dy^{3+} ions were 1–25 at% of Gd^{3+} ions in Ba_2GdNbO_6 host. Stoichiometric amounts of Gd_2O_3, Nb_2O_5, $Ba(NO_3)_2$, Eu_2O_3, Dy_2O_3 were thoroughly mixed and ground using an agate mortar and pestle. During this process, a small amount of ethanol was added in order to mix the materials homogeneously. The samples were fired three times in Al_2O_3 crucibles at 1200 °C for 8 h. Between firings, the samples were reground. After the last firing and grinding, all samples were annealed at 1000 °C for 4 h to eliminate surface defects.

The X-ray diffraction (XRD) measurements were carried out on a Rigaku-Dmax 2500 diffractometer using Cu-$K\alpha$ radiation ($\lambda = 0.15405$ nm). The morphologies of the samples were inspected using a field emission scanning electron microscope (FE-SEM, XL30, Philips). The excitation and emission spectra were taken on an F-4500 spectrophotometer equipped with a 150 W xenon lamp as the excitation source. The luminescence decay curves were obtained from a Lecroy Wave Runner 6100 Digital Oscilloscope (1 GHZ) using a 254 nm laser (pulse width = 4 ns, gate = 50 ns) as the excitation (Continuum Sunlite, OPO). All the measurements were performed at room temperature (RT).

3. Results and discussion

3.1. Phase formation

Fig. 1 shows the XRD patterns of the $Ba_2Gd_{0.9}NbO_6$: $0.10Eu^{3+}$ (Fig. 1a) and Li^+-doped $Ba_2Gd_{0.9}NbO_6$: $0.10Eu^{3+}$ (Fig. 1b) samples as well as that for the standard Ba_2GdNbO_6 (JCPDS Card No. 47-0378). The results of XRD indicate that all the diffraction peaks of Eu^{3+}-doped and Eu^{3+}/Li^+-co-doped samples can be exactly assigned to the standard data of Ba_2GdNbO_6 (JCPDS Card No. 47-0378). No second phase was detected, indicating that the Eu^{3+} ions have been successfully dissolved in the Ba_2GdNbO_6 host lattices by substitution for the Gd^{3+} ions. As shown in Fig. 1b, all the peak intensities for Li^+-doped sample are higher than those for the sample without Li^+ doping (Fig. 1a), indicating that the crystallinity of the Li^+-doped Ba_2GdNbO_6: $0.10Eu^{3+}$ is higher than that of Ba_2GdNbO_6: $0.10Eu^{3+}$ sample. This is of great importance for phosphors, since high crystallinity always means few defects and stronger luminescence. For the Li^+-doped sample, the Li^+ ions incorporated into the host lattice may play a role to promote the crystallinity effectively [18]. The results for $Ba_2Gd_{0.95}NbO_6$: $0.05Dy^{3+}$ and Li^+-doped $Ba_2Gd_{0.95}NbO_6$: $0.05Dy^{3+}$ are similar to those of $Ba_2Gd_{0.9}NbO_6$: $0.10Eu^{3+}$ and Li^+-doped $Ba_2Gd_{0.9}NbO_6$: $0.10Eu^{3+}$, respectively. Fig. 2 exhibits the crystal structure of Ba_2GdNbO_6, which belongs to the cubic crystal system with a space group of *Fm*-3*m*, and there are four Ba_2GdNbO_6 formulas in unit cell ($Z = 4$). The calculated lattice constants, $a = b = c = 8.465$ Å for Ba_2GdNbO_6: $0.10Eu^{3+}$ and $a = b = c = 8.478$ Å for Ba_2GdNbO_6: $0.05Dy^{3+}$, are well compatible with the literature values of $a = b = c = 8.490$ Å for Ba_2GdNbO_6 (JCPDS 47-0378).

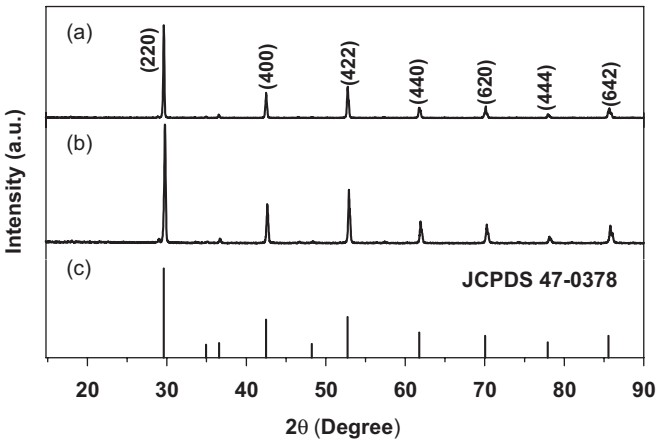

Fig. 1. X-ray diffraction patterns for $Ba_2Gd_{0.9}NbO_6$: $0.10Eu^{3+}$ (a) and Li^+-doped $Ba_2Gd_{0.9}NbO_6$: $0.10Eu^{3+}$ (b) samples, as well as the standard data for Ba_2GdNbO_6 (JCPDS No. 47-0378) (as reference) (c).

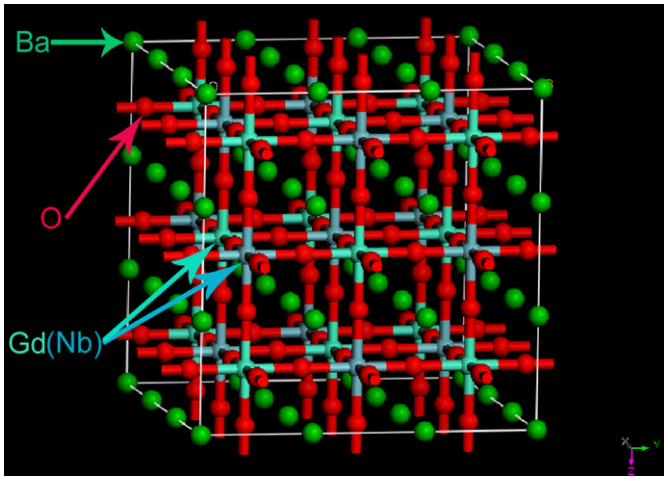

Fig. 2. The crystal structure for Ba_2GdNbO_6.

The crystallite size of the samples can be estimated from the Scherrer equation, $D = 0.941\lambda/\beta\cos\theta$, where D is the average grain size, λ is the X-ray wavelength (0.15405 nm), θ and β are the diffraction angle and full width at half maximum (FWHM) of an observed peak, respectively [26]. The strongest peak (2 2 0) at $2\theta = 29.921^\circ$ was used to calculate the average crystallite size (D) of the Ba_2GdNbO_6: $0.10Eu^{3+}$ particles. The estimated average crystallite size is about 44.6 nm. While for the Li^+-doped Ba_2GdNbO_6: $0.10Eu^{3+}$ sample, the strongest peak (2 2 0) is $2\theta = 29.780^\circ$ and the average crystallite size is about 63.3 nm. From the above crystallite size calculation, we can see that the incorporation of Li^+ ions into the $Ba_2Gd_{0.9}NbO_6$: $0.10Eu^{3+}$ has enlarged the crystallite size.

Fig. 3 shows the FE-SEM micrographs of the Ba_2GdNbO_6: $0.10Eu^{3+}$ (Fig. 3a) and Li^+-doped Ba_2GdNbO_6: $0.10Eu^{3+}$ (Fig. 3b) samples. It is shown that the incorporation of Li^+ has increased the particle grain size (Fig. 3b). It is common that the higher crystallinity leads to the larger crystallite and grain size. The FE-SEM micrographs of the Ba_2GdNbO_6: $0.10Eu^{3+}$ and Li^+-doped Ba_2GdNbO_6: $0.10Eu^{3+}$ samples are in good agreement with the XRD analysis. It is also suggested that the Li^+ ions may serve as a self-promoter for better crystallization or as a lubricant for the complete incorporation of the Eu^{3+} ions into the Ba_2GdNbO_6 hosts [18,27].

3.2. Photoluminescence properties

3.2.1. Ba_2GdNbO_6: Eu^{3+}/Dy^{3+} phosphors

Fig. 4 shows the excitation and emission spectra of the $Ba_2Gd_{0.9}NbO_6$: $0.10Eu^{3+}$ (Fig. 4a,b) and $Ba_2Gd_{0.95}NbO_6$: $0.05Dy^{3+}$ (Fig. 4c,d) samples. Under the 279 nm excitation, the $Ba_2Gd_{0.90}NbO_6$: $0.10Eu^{3+}$ samples exhibit a strong red-orange luminescence. The excitation spectrum (Fig. 4a) monitored by Eu^{3+} $^5D_0$–$^7F_1$ at 593 nm consists of a broad band with a maximum at 279 nm and some narrow excitation peaks at 398 nm ($^7F_0$–$^5L_6$), 467 nm ($^7F_0$–$^5D_2$), 531 and 536 nm ($^7F_0$–$^5D_1$) due to the f–f transitions of

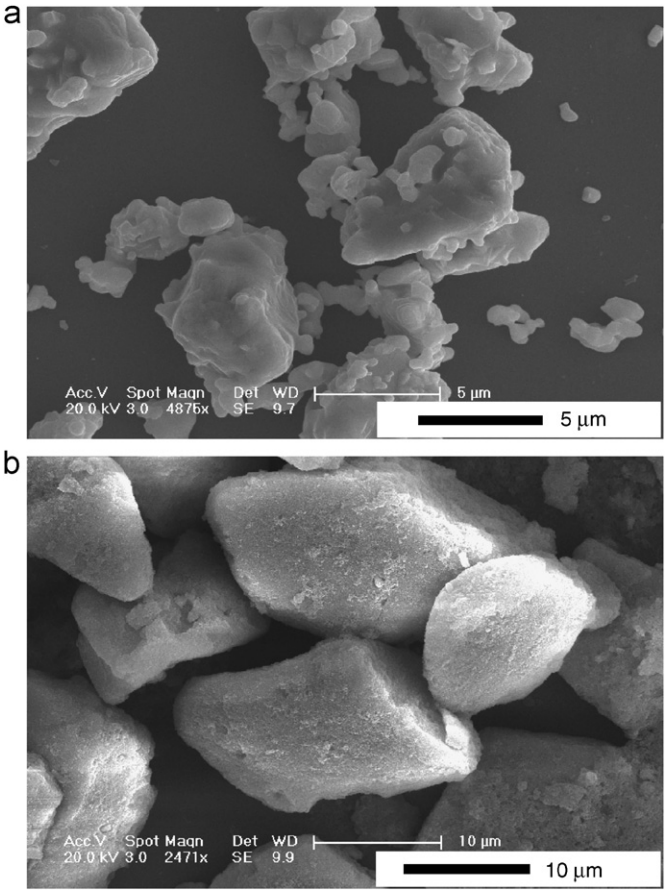

Fig. 3. FE-SEM micrographs of the $Ba_2Gd_{0.9}NbO_6$: $0.10Eu^{3+}$ (a) and Li^+-doped $Ba_2Gd_{0.9}NbO_6$: $0.10Eu^{3+}$ (b) samples.

Eu^{3+} [10]. The strong broad band at 279 nm is attributed to the charge transfer band (CTB) of Eu^{3+}–O^{2-}. The emission spectrum (Fig. 3b) obtained by excitation with 279 nm contains exclusively the characteristic emission of Eu^{3+}. These line transitions arise from the f–f transition of Eu^{3+}, namely, the $^5D_0$–$^7F_1$ (593 nm), $^5D_0$–$^7F_2$ (613, 640 nm), and $^5D_0$–$^7F_3$ (656 nm), respectively [10]. The emission spectrum is dominated by the magnetic dipole transition of $^5D_0$–$^7F_1$ at 593 nm, indicating that the Eu^{3+} ions are located at sites with inversion symmetry in Ba_2GdNbO_6 host lattices. It is well known that the $^5D_0$–$^7F_2$ red emission of Eu^{3+} ions belong to hypersensitive transitions with $\Delta J = 2$, which is strongly influenced by the outside surroundings and can be served as a very efficient and sensitive structural probe [13,28,29]. When Eu^{3+} ions are located at high symmetry local sites (with inversion symmetry center) [28,30], the $^5D_0$–$^7F_2$ emission is usually weaker than the $^5D_0$–$^7F_1$ emission in the spectrum. Fig. 2 shows the ordered perovskite structure of the Ba_2GdNbO_6 crystal. The unit cell of the crystal is a cube divided into eight smaller cubes. The Ba^{2+} ions are located at the corners of the smaller cubes, the O^{2-} ions are positioned at the middle of the sides of the small cubes and the alternating Gd^{3+} and Nb^{5+} ions are positioned in the center of the smaller cubes. On the basis of magnetic

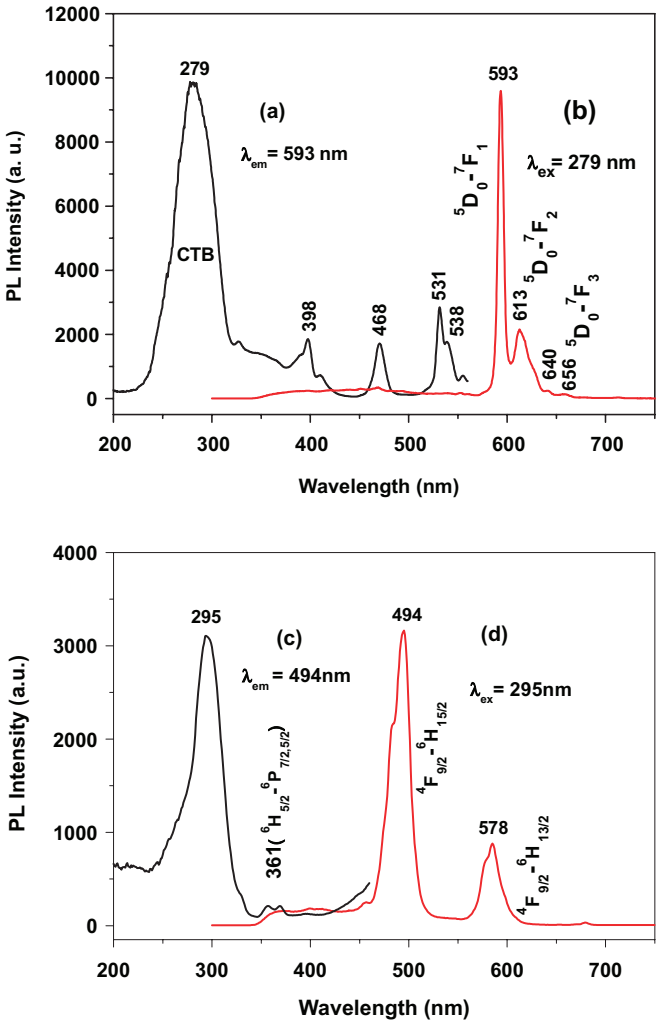

Fig. 4. Excitation and emission spectra of the $Ba_2Gd_{0.9}NbO_6$: $0.10Eu^{3+}$ (a, b) and $Ba_2Gd_{0.95}NbO_6$: $0.05Dy^{3+}$ (c, d) phosphors.

measurements, Division et al. [31] concluded that the Gd^{3+} and Nb^{5+} ions occupied their sites in a random fashion. Obviously, the doped Eu^{3+} (or Dy^{3+}) ions prefer to occupy the Gd^{3+} sites with high symmetry (O_h), based on their close ionic radii [r (Eu^{3+}) = 1.087 Å, r (Gd^{3+}) = 1.078 Å, r (Dy^{3+}) = 0.912 Å] and valence state (+3) in Ba_2GdNbO_6. So, the Eu^{3+} (or Dy^{3+}) site also possesses inversion symmetry in Ba_2GdNbO_6 host. Thus, it is understandable that the magnetic dipole transition $^5D_0$–$^7F_1$ of Eu^{3+} (and $^4F_{9/2}$–$^6H_{15/2}$ of Dy^{3+}, next section) dominate in their emission spectra [5].

The excitation spectrum of $Ba_2Gd_{0.95}NbO_6$: $0.05Dy^{3+}$ (Fig. 4c) monitored by Dy^{3+} $^4F_{9/2}$–$^6H_{15/2}$–$^6H_{15/2}$ transition at 494 nm shows a broad band from 200 to 370 nm with a maximum at 295 nm and a weak line at 361 nm, which correspond to the host lattice absorption due to charge transfer from O^{2-} to Nb^{5+} [32,33] and the characteristic f–f transition ($^6H_{5/2}$–$^6P_{7/2,5/2}$) of Dy^{3+}, respectively. Under the excitation of 295 nm, the $Ba_2Gd_{0.95}NbO_6$: $0.05Dy^{3+}$ samples show a strong whitish blue luminescence. Fig. 4d shows the emission spectrum of $Ba_2Gd_{0.95}NbO_6$: $0.05Dy^{3+}$, which contains exclusively the characteristic emission of Dy^{3+}. The characteristic emission of Dy^{3+} is dominated by two main groups of lines in the blue region (460–505 nm) and yellow region (570–600 nm) corresponding to the transition from $^4F_{9/2}$ to $^6H_{15/2}$, $^6H_{13/2}$ of Dy^{3+}, respectively [5]. The emission spectrum is dominated by the blue emission $^4F_{9/2}$–$^6H_{15/2}$ because the Dy^{3+} ions occupy sites with inversion symmetry (O_h) like Eu^{3+} in Ba_2GdNbO_6 host [5].

The whitish blue color of Dy^{3+} emission and red-orange color of Eu^{3+} emission in Ba_2GdNbO_6 host can be further confirmed by the CIE (Commission Internationale de I'Eclairage 1931 chromaticity) coordinates for the emission spectra of Li^+-doped $Ba_2Gd_{0.95}NbO_6$: $0.05Dy^{3+}$ (x = 0.2060, y = 0.2740), $Ba_2Gd_{0.95}NbO_6$: $0.05Dy^{3+}$ (x = 0.2237, y = 0.3201), $Ba_2Gd_{0.9}NbO_6$: $0.10Eu^{3+}$ (x = 0.5084, y = 3497) and Li^+-doped $Ba_2Gd_{0.9}NbO_6$: $0.10Eu^{3+}$ (x = 0.5247, y = 0.3488), as shown, respectively, in points a, b (whitish blue region) and c, d (red-orange region) in Fig. 5.

To determine the compositions with the highest photoluminescence (PL) intensity, we varied the doping contents of Eu^{3+}, Dy^{3+} ions in Ba_2GdNbO_6. Fig. 6a, b, respectively, shows the dependence of the emission intensities of the Eu^{3+}, Dy^{3+} ions on their doping concentrations (x, y) in $Ba_2Gd_{1-x}NbO_6$: xEu^{3+} (Fig. 6a) and $Ba_2Gd_{1-y}NbO_6$: yDy^{3+} (Fig. 6b). It can be seen that the emission intensities of Eu^{3+}, Dy^{3+} ions increase with increase is their doping concentrations (x, y) first, reaching the highest value at x = 0.10, y = 0.05, respectively, and then decrease with

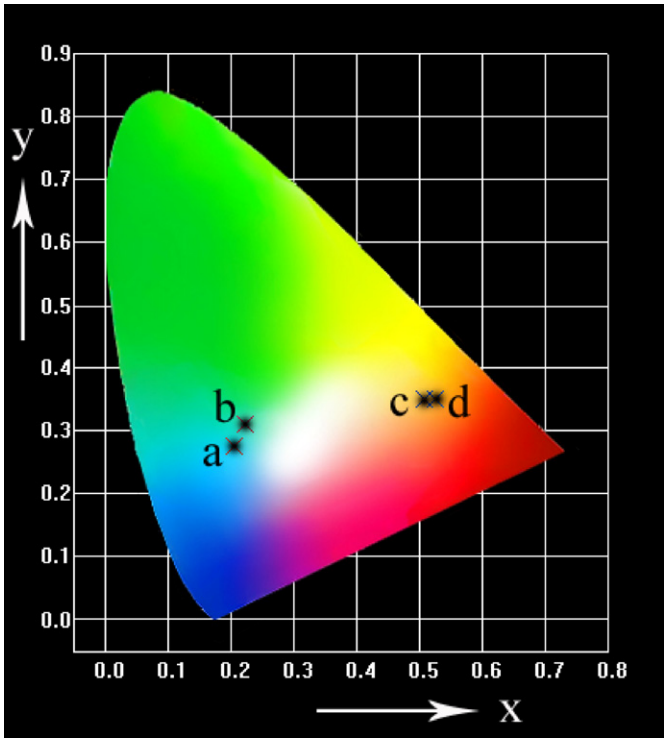

Fig. 5. The CIE chromaticity diagram for Li^+-doped $Ba_2Gd_{0.95}NbO_6$: $0.05Dy^{3+}$ (a), $Ba_2Gd_{0.95}NbO_6$: $0.05Dy^{3+}$ (b), $Ba_2Gd_{0.9}NbO_6$: $0.10Eu^{3+}$ (c) and Li^+-doped $Ba_2Gd_{0.9}NbO_6$: $0.10Eu^{3+}$ (d).

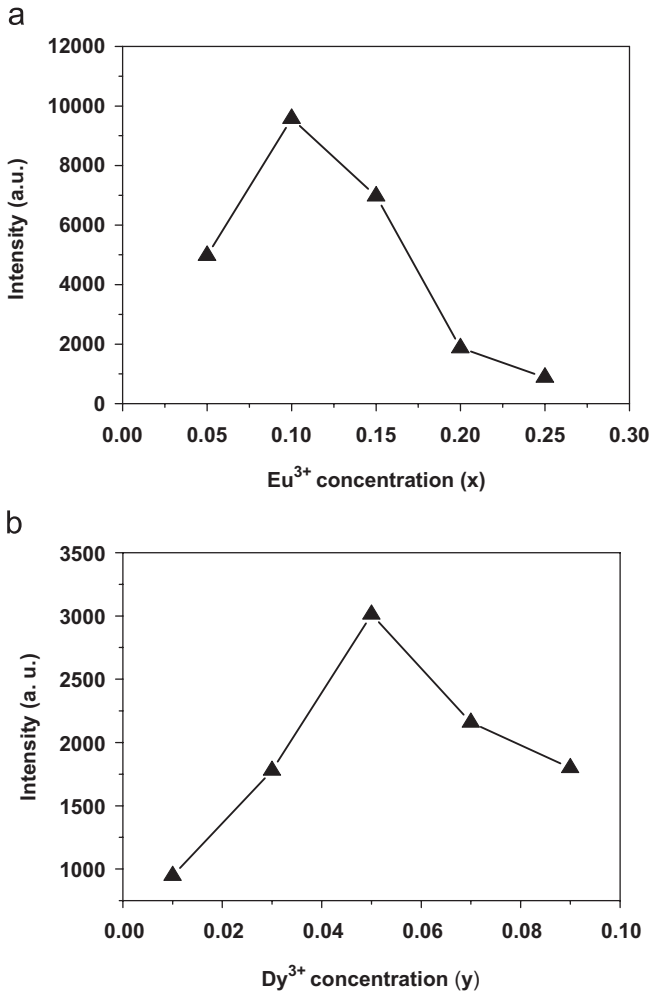

Fig. 6. The photoluminescence emission intensity of Eu^{3+} ($^5D_0$–$^7F_1$) and Dy^{3+} ($^4F_{9/2}$–$^6H_{15/2}$–$^6H_{15/2}$) ions as a function of their doping concentrations (x, y) in (a) $Ba_2Gd_{1-x}NbO_6$: xEu^{3+} and (b) $Ba_2Gd_{1-y}NbO_6$: yDy^{3+} samples.

increase their contents (x, y) due to the concentration quenching effect [34]. Thus, the optimum concentration for Eu^{3+} ions is determined to be 10 at% of Gd^{3+} and that for Dy^{3+} ions is 5 at% of Gd^{3+} in the Ba_2GdNbO_6 host. The concentration quenching of Dy^{3+} luminescence is mainly caused by cross-relaxation, i.e., energy transfer among Dy^{3+} ions, for example, $Dy^{3+}(^4F_{9/2}) + Dy^{3+}(^6H_{15/2}) \rightarrow Dy^{3+}(^6F_{3/2}) + Dy^{3+}(^6F_{11/2})$ [10,13,35]. Because the luminescence quenching is caused by the energy transfer among the same rare earth ions, the critical distance (R_c) can be estimated in terms of the equation, $R_c = 2(3V/4\pi X_c N)^{1/3}$ (where V is the volume of the unit cell, X_c is the critical concentration and N is the number of available crystallographic sites occupied by the activator ions in the unit cell [36]. Based on the related crystal parameters (V, Z and N) of the phosphors [37,38], the corresponding R_c (Eu^{3+}–Eu^{3+}) value for $Ba_2Gd_{0.9}NbO_6$: $0.10Eu^{3+}$ and R_c (Dy^{3+}–Dy^{3+}) value for $Ba_2Gd_{0.95}NbO_6$: $0.05Dy^{3+}$ are determined to be 0.4876 and 0.3870 nm, respectively.

3.2.2. Li^+-doping effects

Fig. 7a–d show the typical PL spectra of the Ba_2GdNbO_6: Eu^{3+}/Dy^{3+} and the Li^+-doped Ba_2GdNbO_6: Eu^{3+}/Dy^{3+}, respectively. Besides different emission intensities, the spectra have identical shape. The PL intensities of the Li^+-doped Ba_2GdNbO_6: Eu^{3+} and Ba_2GdNbO_6: Dy^{3+} are higher than those of the $Ba_2Gd_{0.9}NbO_6$: $0.10Eu^{3+}$ and $Ba_2Gd_{0.95}NbO_6$: $0.05Dy^{3+}$, respectively. By varying the contents of Li^+ ions in Ba_2GdNbO_6: Eu^{3+}/Dy^{3+}, we determined the compositions with the highest emission intensity. Figs. 8a, b show the dependence of the emission intensity of Li^+ on its doping concentration (x) in $Ba_2Gd_{0.9}Eu_{0.1}NbO_6$: xLi^+ (Fig. 8a) and $Ba_2Gd_{0.95}Dy_{0.05}NbO_6$: yLi^+ (Fig. 8b) samples, respectively. As seen clearly from Fig. 8a, the emission intensity of Eu^{3+} increases with increase in Li^+ concentrations (x) first, reaching a maximum value at $x = 0.01$ and then decreases with increasing contents (y). Thus, the optimum concentration for Li^+ is 0.01 in the $Ba_2Gd_{0.9}Eu_{0.1}NbO_6$: xLi^+ sample. The same situation holds for $Ba_2Gd_{0.95}Dy_{0.05}NbO_6$: yLi^+, and the optimum concentration for Li^+ is 0.07 in the

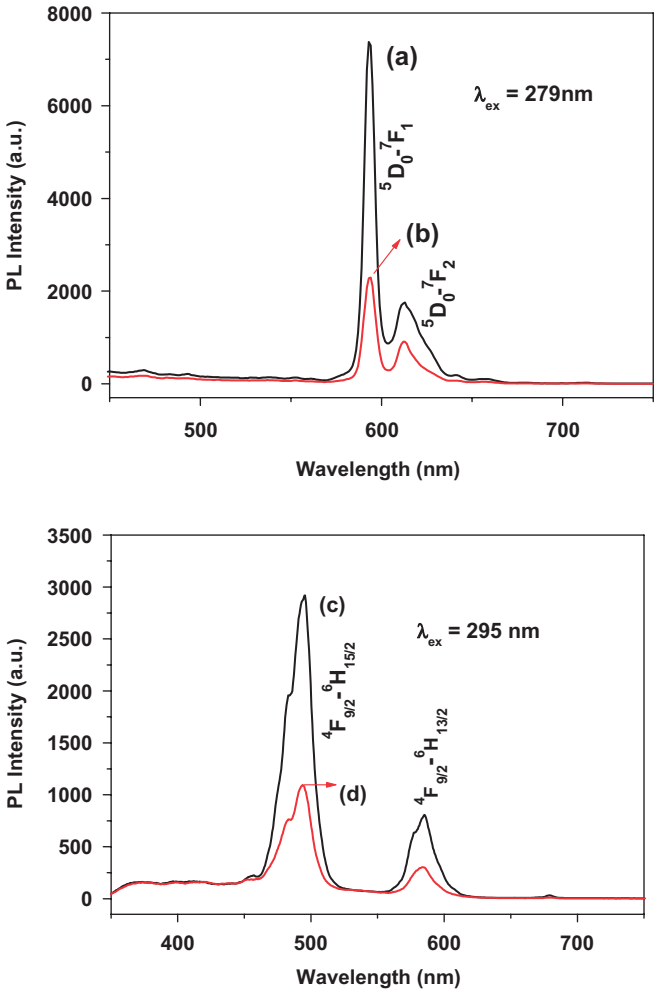

Fig. 7. A comparison of the PL spectra for the $Ba_2Gd_{0.9}NbO_6$: $0.10Eu^{3+}$, $0.01Li^+$ (a) and $Ba_2Gd_{0.9}NbO_6$: $0.1Eu^{3+}$ (b), $Ba_2Gd_{0.95}NbO_6$: $0.05Dy^{3+}$, $0.07Li^+$ (c) and $Ba_2Gd_{0.95}NbO_6$: $0.05Dy^{3+}$ (d).

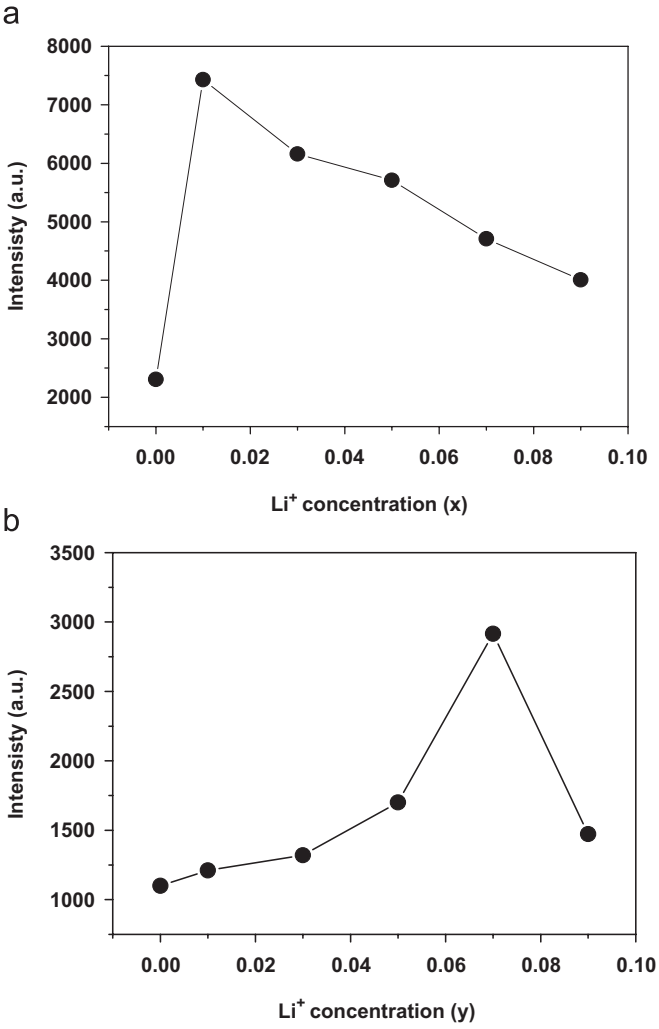

Fig. 8. The PL emission intensity of the Eu^{3+} and Dy^{3+} in the Ba_2GdNbO_6 $0.10Eu^{3+}$, xLi^+ (a) and Ba_2GdNbO_6: $0.05Dy^{3+}$, yLi^+ (b) as a function of the concentration (x, y) of Li^+ ions.

$Ba_2Gd_{0.95}Dy_{0.05}NbO_6$: yLi^+ sample. At low Li^+ ion concentration, the Li^+ ions may serve as a self-promoter for better crystallization or as a lubricant for the complete incorporation of the Eu^{3+} and Dy^{3+} ions into the Ba_2GdNbO_6 lattice during the sintering process and thus they enhance the PL intensity [18,28]. While at higher Li^+-ions concentration, many defects may be induced in the systems that are bad for the photoluminescence, which results in decrease of PL intensity [20].

A sample model illustrating the excitation and emission process in Ba_2GdNbO_6: Eu^{3+}/Dy^{3+} and Li^+-doped Ba_2GdNbO_6: Eu^{3+}/Dy^{3+} is shown in Fig. 9. In Ba_2GdNbO_6: Eu^{3+} and Li^+-doped Ba_2GdNbO_6: Eu^{3+}, the excitation (279 nm) takes place on the CTB of Eu^{3+}–O^{2-}, then the excitation energy relaxes to the $^5D_0$ energy level of Eu^{3+}, where the radiative transitions to ground state ($^7F_1$, $^7F_2$) occur, resulting in $^5D_0$–$^7F_1$ (593 nm) and $^5D_0$–$^7F_2$ (613 nm) emission, as shown in Fig. 9 (left). However, in Ba_2GdNbO_6: Dy^{3+} and Li^+-doped Ba_2GdNbO_6: Dy^{3+},

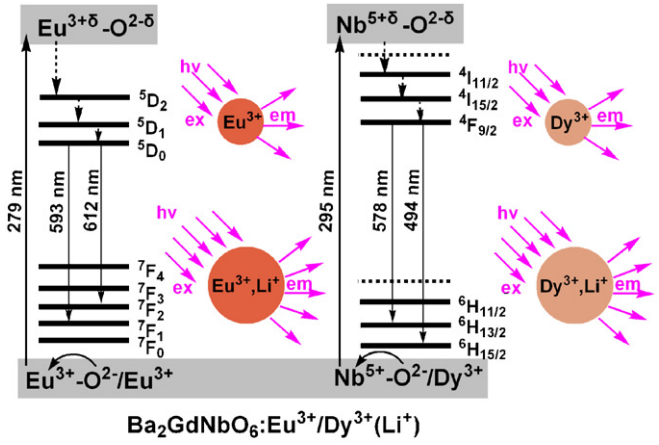

Fig. 9. A simple model illustrating excitation and emission process in Ba_2GdNbO_6: Eu^{3+}/Dy^{3+} and how Li^+-doping can improve the PL intensity of the $Ba_2Gd_{0.9}NbO_6$: Eu^{3+}/Dy^{3+} phosphors.

the excitation (295 nm) is mainly on the CTB of Nb^{5+}–O^{2-} (the CTB of Dy^{3+}–O^{2-} is located at much high energy below 200 nm, which is not easy to take place), then the excitation energy is transferred to the excited state ($^4F_{9/2}$ level) of Dy^{3+}, in which radiative transition takes place, resulting in the $^4F_{9/2}$–$^6H_{15/2}$ and $^4F_{9/2}$–$^6H_{13/2}$ emissions of Dy^{3+}, as shown in Fig. 9 (right), due to the higher crystallinity and larger grain size of the Li^+-doped Ba_2GdNbO_6: Eu^{3+}/Dy^{3+} phosphors (the particles are denoted as color balls with different sizes in Fig. 9). The Li^+-doped Ba_2GdNbO_6: Eu^{3+}/Dy^{3+} phosphor particles (larger size with higher crystallinity and less defects) can be excited by more photons than the Ba_2GdNbO_6: Eu^{3+}/Dy^{3+} phosphor (smaller size with lower crystallinity and more defects) under the same excitation conditions, and more photons will emit in the former than in the latter. Thus, it is understandable that the Li^+-doped Ba_2GdNbO_6: Eu^{3+}/Dy^{3+} phosphors have higher photoluminescence intensity than that of the Ba_2GdNbO_6: Eu^{3+}/Dy^{3+} phosphors.

Fig. 10 shows the luminescence decay curves for Ba_2GdNbO_6: $0.10Eu^{3+}$ (a), Ba_2GdNbO_6: $0.10Eu^{3+}$, $0.10Li^+$ (b), Ba_2GdNbO_6: $0.05Dy^{3+}$ (c) and Ba_2GdNbO_6: $0.05Dy^{3+}$, $0.07Li^+$ (d), respectively. In general, these decay curves for the Eu^{3+} (593 nm, $^5D_0$–$^7F_1$) and Dy^{3+} (494 nm, $^4F_{9/2}$–$^6H_{15/2}$) in Ba_2GdNbO_6 can be well fitted into a single exponential function as $I = I_0 \exp(-t/\tau)$ (here I_0 is the initial emission intensity at $t = 0$ and τ is the $1/e$ lifetime of the emission center). The lifetimes of Eu^{3+} ($^5D_0$ excited state) and Dy^{3+} ($^4F_{9/2}$ excited state) in Ba_2GdNbO_6: $0.10Eu^{3+}$, Ba_2GdNbO_6: $0.10Eu^{3+}$, $0.10Li^+$, Ba_2GdNbO_6: $0.05Dy^{3+}$, Ba_2GdNbO_6: $0.05Dy^{3+}$, $0.07Li^+$ were determined as 2.26, 2.29, 0.71 and 0.58 ms, respectively. These values are basically in agreement with those reported in Refs. [5,39]. It indicates that the incorporation of Li^+ ions into the host has less effect on the decay behavior and lifetime values of Eu^{3+} and Dy^{3+}.

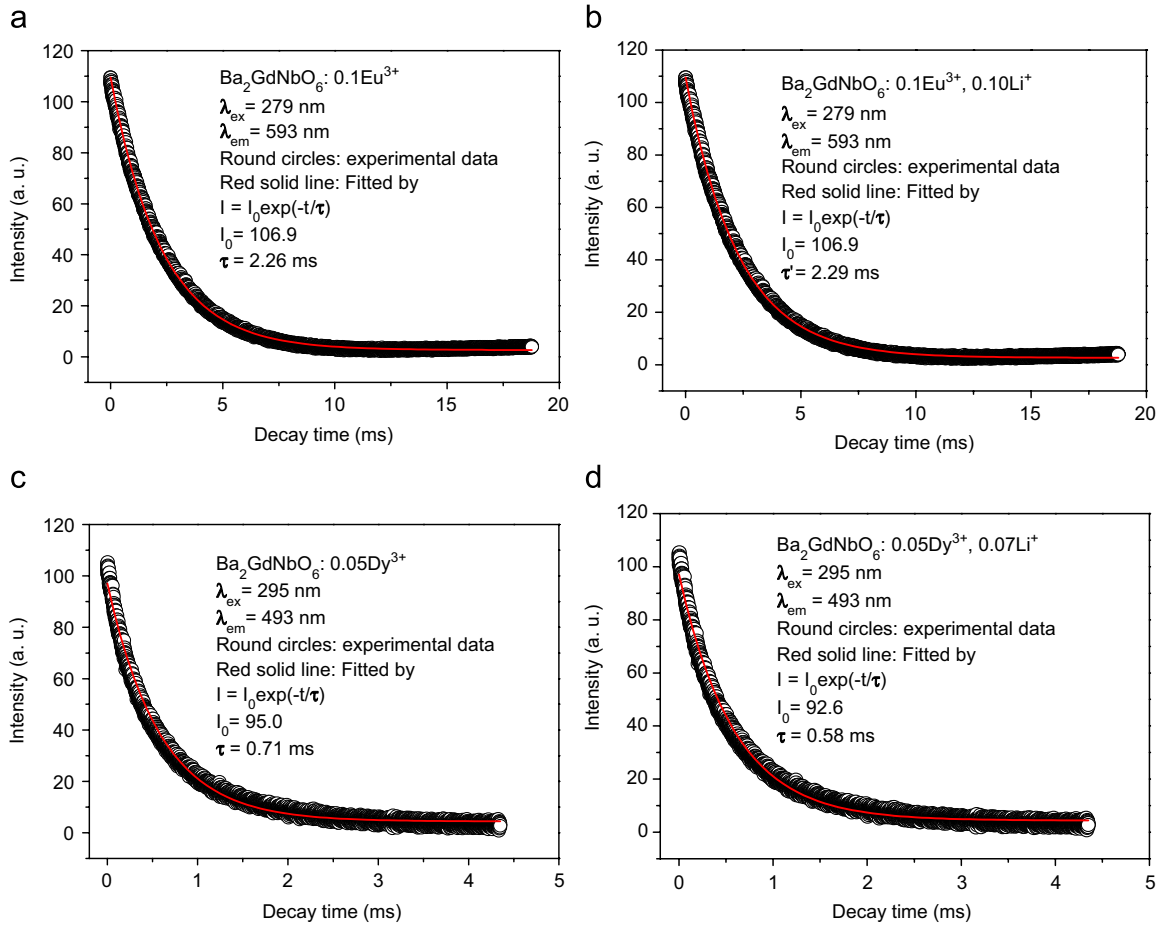

Fig. 10. The luminescence decay curves for Eu^{3+} in Ba_2GdNbO_6: $0.10Eu^{3+}$ (a) Ba_2GdNbO_6: $0.10Eu^{3+}$, $0.10Li^{+}$ (b), Dy^{3+} in Ba_2GdNbO_6: $0.05Dy^{3+}$ (c) and Ba_2GdNbO_6: $0.05Dy^{3+}$, $0.07Li^{+}$ (d).

4. Conclusions

Ba_2GdNbO_6: Eu^{3+}/Dy^{3+} and Li^{+}-doped Ba_2GdNbO_6: Eu^{3+}/Dy^{3+} phosphors were prepared by solid-state reaction and their luminescent properties were investigated. Under the excitation of 279 or 295 nm, the Ba_2GdNbO_6: Eu^{3+} and Ba_2GdNbO_6: Dy^{3+} phosphors show the red-orange emission from Eu^{3+} and whitish blue emission from Dy^{3+}, respectively. Due to the existence of an inversion symmetry for the sites occupied by Eu^{3+} and Dy^{3+} in Ba_2GdNbO_6 host, the $^5D_0$–$^7F_1$ transition of Eu^{3+} and $^4F_{9/2}$–$^6H_{15/2}$ transition of Dy^{3+} dominate their emission spectra, respectively. Effective excitation can be realized on Eu^{3+} via Eu^{3+}–O^{2-} charge transfer transition and on Dy^{3+} via Nb^{5+}–O^{2-} charge transfer transition, respectively. The optimum concentrations (x) for Eu^{3+} and Dy^{3+} in $Ba_2Gd_{(1-x)}NbO_6$: xEu^{3+}/Dy^{3+} samples are determined to be $x = 0.10$ (Eu^{3+}) and 0.05 (Dy^{3+}), respectively. Suitable amount incorporation of Li^{+} ions in the phosphors can promote the crystallinity and increase the grain size to a great extent, and thus enhance the PL emission intensity greatly. The method might be used for other phosphors to enhance their emission intensity.

Acknowledgments

This project is financially supported by the foundation of "Bairen Jihua" of Chinese Academy of Sciences, the National Natural Science Foundation of China (50572103, 20431030, 00610227) and the MOST of China (Nos. 2003CB314707, 2007CB935502). Dr M. Yu is grateful for the special starting research fund for the Awardees of President Prize of Chinese Academy of Sciences (2005–2007).

References

[1] M.L. Pang, J. Lin, J. Fu, Z.Y. Cheng, Mater. Res. Bull. 39 (2004) 1607.
[2] M.L. Pang, J. Lin, J. Cryst. Growth 284 (2005) 262.
[3] J. Thomas, N. Hans, R. Cees, Angew. Chem. Int. Ed. 37 (1998) 3084.
[4] C.K. Lin, M.L. Pang, M. Yu, J. Lin, J. Lumin. 114 (2005) 299.
[5] W.Y. Shen, M.L. Pang, J. Lin, J.Y. Fang, J. Electrochem. Soc. 152 (2005) H25.
[6] Z.L. Fu, S.H. Zhou, Y.N. Yu, S.Y. Zhang, J. Phys. Chem. B 109 (2005) 23320.
[7] P. Nemec, P. Maly, J. Appl. Phys. 87 (2000) 3342.
[8] A.A. Bol, A. Meijerink, J. Lumin. 87 (2000) 315.
[9] E. Loh, Phys. Rev. 147 (1966) 332.

[10] G. Blasse, B.C. Grabmaier, Luminescent Materials, Springer, Berlin/Heidelberg, 1994.
[11] J.L. Sommerdijk, A. Bril, F.M.J.H. Hoex-Strik, Philips Res. Rep. 32 (1977) 149.
[12] J. Lin, Q. Su, J. Alloys Compds. 210 (1994) 159.
[13] J. Kurian, K.V.O. Nair, P.K. Sajith, A.M. John, J. Koshy, Appl. Superconduct. 6 (1998) 259.
[14] W.T. Fu, D.J.W. IJdo, J. Solid State Chem. 179 (2006) 1022.
[15] J. Kurian, P.R.S. Waiar, P.K. Sajith, J. Koshy, J. Superconduct. 11 (1998) 683.
[16] G. Blasse, A. Bril, Philips Tech. Tijdscrift 31 (1970) 314.
[17] O. Visser, L. Visscher, P.J.G. Aeris, W.C. Nieuwpoort, J. Chem. Phys. 96 (1992) 4.
[18] S. Yi, J.S. Bae, K.S. Shim, J.H. Jeong, J.C. Park, P.H. Holloway, Appl. Phys. Lett. 84 (2004) 353.
[19] H. Jang, D. Jeon, Appl. Phys. Lett. 90 (2007) 041906.
[20] M.L. Pang, W.Y. Shen, J. Lin, J. Appl. Phys. 97 (2005) 033511.
[21] J. Thomas, N. Hans, R. Cees, Angew. Chem. Int. Ed. 37 (1998) 3084.
[22] C.K. Lin, M.L. Pang, M. Yu, J. Lin, J. Lumin. 114 (2005) 299.
[23] K.A. Hyeon, S.H. Byeon, J.C. Park, D.K. Kim, K.S. Suh, Solid State Commun. 115 (2000) 99.
[24] J.C. Park, H.K. Moon, D.K. Kim, S.H. Byeon, B.C. Kim, K.S. Suh, Appl. Phys. Lett. 77 (2000) 2162.
[25] K.C. Misbra, J.K. Berkowitz, K.H. Johnson, P.C. Schmidt, Phys. Rev. B 45 (1992) 10902.
[26] Y.W. Zhang, S. Jin, S.J. Tian, G.B. Li, T. Jia, C.S. Liao, C.H. Yan, Chem. Mater. 13 (2001) 372.
[27] S. Yi, J.S. Bae, B.K. Moon, J.H. Jeong, J.C. Park, W. Kim, Appl. Phys. Lett. 81 (2002) 3344.
[28] Q. Su, Z. Pei, L. Chi, H. Zhang, F. Zou, J. Alloys Compds. 192 (1993) 25.
[29] J.M. Nedelec, D. Avignant, R. Mahiou, Chem. Mater. 14 (2002) 651.
[30] L.C. Courrol, L. Gomes, A. Brenier, C. Pedrini, C. Madej, G. Boulon, Radiat. Eff. Defects Solids. 135 (1995) 81.
[31] R. Division, E.I.P. Nemours, W. Delaware, J. Inorg. Nucl. Chem. 15 (1960) 352.
[32] X.M. Liu, J. Lin, J. Appl. Phys. 100 (2006) 1.
[33] F. Gu, S.F. Wang, M.K. Lü, G.J. Zhou, S.W. Liu, D. Xu, D.R. Yuan, Chem. Phys. Lett. 380 (2003) 185.
[34] M.L. Pang, J. Lin, J. Fu, R.B. Xing, C.X. Luo, Y.C. Han, Opt. Mater. 23 (2003) 547.
[35] Z. Xiu, Z. Yang, M. Lü, S. Liu, H. Zhang, G. Zhou, Opt. Mater. 29 (2006) 431.
[36] G. Blasse, Philips Res. Rep. 24 (1969) 131.
[37] S.E. Dali, V.V.S.S. Sunder, M. Jayachandra, M.J. Chockalingan, J. Mater. Sci. Lett. 17 (1998) 619.
[38] M.L. Pang, J. Lin, Z.Y. Cheng, J. Fu, R.B. Xing, S.B. Wang, Mater. Sci. Eng. B 100 (2003) 124.
[39] P.Y. Jia, J. Lin, X.M. Han, M. Yu, Thin Solid Films 483 (2005) 122.